SCIENCE CHINA
Physics, Mechanics & Astronomy

• Article •

October 2024 Vol. 67 No. 10: 100313
https://doi.org/10.1007/s11433-024-2432-9

Quantum weak force sensing with squeezed magnomechanics

Qian Zhang[1†], Jie Wang[1†], Tian-Xiang Lu[5], Ran Huang[2], Franco Nori[2,3,4], and Hui Jing[1,6*]

[1] *Key Laboratory of Low-Dimensional Quantum Structures and Quantum Control of Ministry of Education, Department of Physics and Synergetic Innovation Center for Quantum Effects and Applications, Hunan Normal University, Changsha 410081, China;*
[2] *Theoretical Quantum Physics Laboratory, Cluster for Pioneering Research, RIKEN, Wako-shi 351-0198, Japan;*
[3] *Center for Quantum Computing, RIKEN, Wako-shi 351-0198, Japan;*
[4] *Department of Physics, University of Michigan, Ann Arbor 48109-1040, USA;*
[5] *College of Physics and Electronic Information, Gannan Normal University, Ganzhou 341000, China;*
[6] *Academy for Quantum Science and Technology, Zhengzhou University of Light Industry, Zhengzhou 450002, China*

Received April 13, 2024; accepted June 7, 2024; published online August 1, 2024

Cavity magnomechanics, exhibiting remarkable experimental tunability, rich magnonic nonlinearities, and compatibility with various quantum systems, has witnessed considerable advances in recent years. However, the potential benefits of using cavity magnomechanical (CMM) systems in further improving the performance of quantum-enhanced sensing for weak forces remain largely unexplored. Here we show that, by squeezing the magnons, the performance of a quantum CMM sensor can be significantly enhanced beyond the standard quantum limit (SQL). We find that, for comparable parameters, two orders of magnitude enhancement in the force sensitivity can be achieved in comparison with the case without magnon squeezing. Moreover, we obtain the optimal parameter regimes of homodyne angle for minimizing the added quantum noise. Our findings provide a promising approach for highly tunable and compatible quantum force sensing using hybrid CMM devices, with potential applications ranging from quantum precision measurements to quantum information processing.

quantum force sensing, cavity magnomechanics, magnon Kerr effect

PACS number(s): 42.50.Lc, 71.36.+c, 75.30.Ds, 42.50.Pq, 63.20.Ls

Citation: Q. Zhang, J. Wang, T.-X. Lu, R. Huang, F. Nori, and H. Jing, Quantum weak force sensing with squeezed magnomechanics, Sci. China-Phys. Mech. Astron. **67**, 100313 (2024), https://doi.org/10.1007/s11433-024-2432-9

1 Introduction

Hybrid cavity magnomechanical (CMM) systems [1-6] based on collective spin excitations (i.e., magnons) in ferromagnetic crystals (e.g., yttrium iron garnet YIG) exhibit remarkable experimental tunability and compatibility [7-9], enabling strong and coherent interactions between magnons and photons, phonons, as well as superconducting qubits. These have become a versatile platform for fundamental studies with a wide range of applications, including electromagnetically induced transparency and absorption [10], quantum entanglement [11-14], quantum control of a single magnon [15], nonreciprocal magnon blockade [16], nonclassical states [17-19], magnonic frequency comb [20], quantum parametric amplification [21] and mechanical cooling [22]. In a very recent experiment [23], broken PT-symmetry was achieved via Non-Hermiticity caused by on-site loss, generating complex-valued edge states. Particularly, the YIG

*Corresponding author (email: jinghui73@foxmail.com)
† These authors contributed equally to this work.

sphere, which is rich in Kerr-type nonlinearity due to magnetocrystalline anisotropy [24], has emerged as a promising new tool with extensive applications, such as quantum entanglement [25-28], bi- and multi-stabilities [29-32], ground-state cooling [33, 34], and nonreciprocal effects [35-37].

In parallel, quantum-enhanced sensing with the aid of quantum entanglement or squeezing has been widely used for the measurement of force [38-40], displacement [41], electromagnetic fields [42-44], acceleration [45, 46], single spin [47], mass [48, 49] due to their superior sensitivity to external perturbations. Recently, by using entanglement-enhanced joint force measurements with two optomechanical sensors, the SQL was surpassed scaling for arrayed optomechanical sensors [50]. However, how to achieve sub-SQL quantum force sensing by utilizing the unique advantages of CMM systems has remained unexplored until now.

In this work, we propose to build a bridge between such two active fields as quantum engineering of CMM systems and quantum-enhanced sensing. We show that the performance of a CMM sensor can be significantly enhanced drawing support from the magnon squeezing. We show that by tuning the magnon Kerr strength, the effects of backaction noise can be mitigated [8], allowing for a considerable suppression of quantum noise, two orders of magnitude less noisy (that is, much more sensitive) than the SQL. Moreover, we obtain the optimal parameter regimes of homodyne angle for minimizing the added quantum noise. Our work is compatible with existing CMM techniques, and all parameters used for numerical calculations are experimentally accessible [7, 10].

2 Quantum-enhanced force sensing by squeezing magnons

In recent experiments, CMM devices with remarkable experimental tunability have been utilized to achieve bi- and multi-stability [30, 51], ternary logic gates and long-time memory [31], magnomechanically induced transparency and absorption [10], to name a few [31]. We also note that advanced techniques based on non-classical squeezed light resources been developed to overcome the SQL for individual sensors [50, 52, 53]. Note that the merits of the CMM system in generating quantum squeezing have already been confirmed in experiments [18]. However, as far as we know, the possibility of enhancing weak force sensing by utilizing squeezed CMM system has not been explored.

Here we consider a hybrid CMM system, as sketched in Figure 1(a). The strong coupling between microwave photons and magnons generated by a ferromagnetic YIG sphere placed inside the cavity is achieved via the magnetic dipole interaction, and can be adjusted by varying the position of the YIG sphere inside the cavity [10]. The magnetostrictive force couples magnons and phonons [4, 54-56]. The optomechanical interaction is neglected given that the size of the YIG sphere (0.1-1 mm) is much smaller than the wavelength of the microwave field. In the frame rotating at the drive frequency ω_d, the Hamiltonian of the system can be described as

$$H = \hbar\Delta_c a^\dagger a + \hbar\Delta_m m^\dagger m + \frac{\hbar}{2}\omega_b\left(Q^2+P^2\right) + \hbar g_{\rm mb} m^\dagger m Q + \hbar g_{\rm ma}\left(a^\dagger m + a m^\dagger\right) + K m^\dagger m m^\dagger m + i\hbar\Omega\left(m^\dagger - m\right), \quad (1)$$

where a ($a^\dagger$) and m ($m^\dagger$) represent the annihilation (creation) operator of the cavity mode (with frequency ω_a) and the magnon mode (with frequency ω_m), respectively; $\Delta_c(\Delta_m) = \omega_a(\omega_m) - \omega_d$ denotes the detuning between the cavity (magnon) mode and the driving magnetic field; Q and P represent the dimensionless position and momentum quadratures of the mechanical mode at the resonance frequency ω_b, satisfying the commutation relation $[Q, P] = i$; $g_{\rm ma}$ and $g_{\rm mb}$ represent the magnon-photon coupling strength and the magnon-phonon coupling strength, respectively; $K = \mu_0 K_{\rm an}\gamma^2/(M^2 V_m)$ is the strength of the magnon Kerr effect caused by the magnetocrystalline anisotropy, where μ_0 is the vacuum permeability; $\gamma = 2\pi \times 28\,\mathrm{GHz/T}$ is the gyromagnetic ration; M is the saturation magnetization; $K_{\rm an}$ and V_m are the first-order anisotropy constant and the volume of the YIG sphere, respectively. Figure 1(b) shows K is inversely proportional to the cube of the diameter D of the YIG sphere; $\Omega = \sqrt{5}\gamma\sqrt{N}B_0/4$ represents strength of the drive magnetic field directly pumping the YIG sphere, where B_0 denotes the amplitude of the drive field; $N = \rho V_m$ denotes the total number of spins with $\rho = 4.22 \times 10^{27}\,\mathrm{m}^{-3}$ is the spin density of the YIG sphere. The YIG sphere is directly driven by a microwave field, unlike the methods in refs. [7, 10], which drive the cavity instead, exerting a weak influence on the magnon subsystem, and thus making it challenging to observe the nonlinear effects [29]. Additionally, since we focus only on the lowest order ferromagnetic resonance mode, and the microwave drive field around the YIG is approximately uniform [7], the impact of the direction or the location of the drive field is neglected.

Note that the CMM system was already well-established in experiments. For example, a strongly coupled cavity-magnon system was utilized for realizing the bi- and multi-stability [30, 51], and by selecting suitable input power, the ternary logic gate and long-time memory were experimentally demonstrated in a hybrid CMM system with the magnon Kerr effect [31]. We also note that, by introducing quantum squeezing or entanglement, an improved sensitivity in the shot-noise-dominant regime was achieved [57], and by tun-

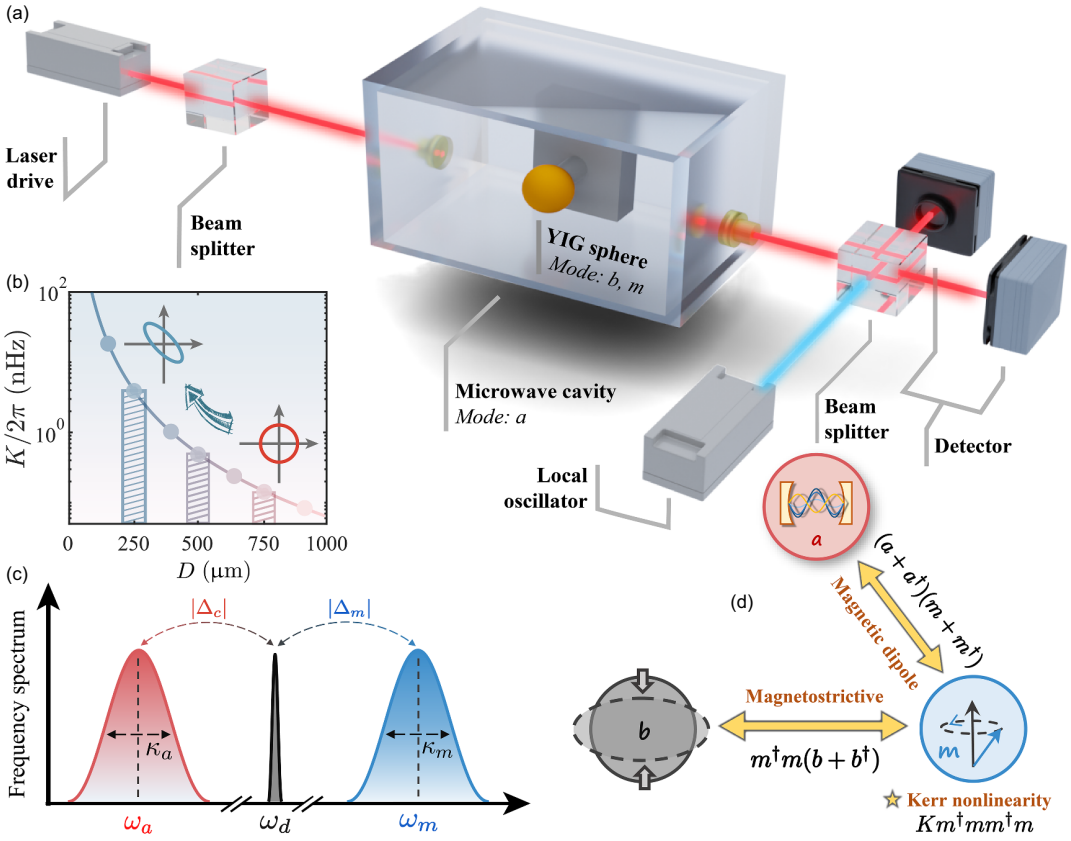

Figure 1 (Color online) (a) Schematic of the hybrid CMM system. Magnon squeezing is achieved by a YIG sphere, which correlates the amplitude and phase fluctuations of the magnon mode. The output light field is measured with a balanced homodyne detector. (b) The magnon Kerr strength K (log scale) is plotted as a function of the diameter D of the YIG sphere [29]. As the diameter D decreases, the magnon Kerr strength K increases (i.e., K is inversely proportional to D). (c) The frequency spectrum and linewidths of the system. The frequency of the drive field is blue detuned by Δ_c from the cavity resonance frequency ω_a, and by Δ_m from the magnon resonance frequency. The linewidths of the cavity mode and the magnon mode are κ_a and κ_m, respectively. (d) Schematic diagram of the different interactions in a hybrid CMM system [4, 10], wherein the magnons couple to photons through magnetic dipole interaction as well as to phonons through magnetostrictive interaction [54]. The optomechanical interaction is neglected given that the size of the YIG sphere (0.1-1 mm) is much smaller than the wavelength of the microwave field.

ing the pump phase of the optical parametric amplifier, considerably suppressed quantum noise and thus giant enhancement of force sensitivities were achieved [39]. Indeed, the merits of the CMM system in generating quantum squeezing have already confirmed in experiments [18], and now our primary objective in this work is to investigate the impact of magnon squeezing on quantum-enhanced weak force sensing.

The quantum Langevin equations (valid when $\omega_a, \omega_m \gg g_{\rm ma}, \kappa_a, \kappa_m$) describing the system are given by

$$\begin{aligned}
\dot{a} &= -\left[i\Delta_c + \frac{\kappa_a}{2}\right]a - ig_{\rm ma}m + \sqrt{\kappa_a}a^{\rm in},\\
\dot{m} &= -\left[i\Delta_m + \frac{\kappa_m}{2}\right]m - ig_{\rm mb}mQ - ig_{\rm ma}a\\
&\quad - 2iKm^\dagger mm + \Omega + \sqrt{\kappa_m}m^{\rm in},\\
\dot{Q} &= \omega_b P, \quad \dot{P} = -\omega_b Q - g_{\rm mb}m^\dagger m - \gamma_b P + \xi^{\rm in},
\end{aligned} \tag{2}$$

where κ_a ($a^{\rm in}$), κ_m ($m^{\rm in}$), and γ_b ($\xi^{\rm in}$) are the dissipation rates (input noise operators) of the cavity, magnon and mechanical modes, respectively. The steady-state mean values are

$$\begin{aligned}
m_s &= \frac{\Omega\left(i\Delta_c + \frac{\kappa_a}{2}\right)}{\left(i\tilde{\Delta}_m + \frac{\kappa_m}{2}\right)\left(i\Delta_c + \frac{\kappa_a}{2}\right) + g_{\rm ma}^2},\\
Q_s &= -\frac{g_{\rm mb}}{\omega_b}|m_s|^2,
\end{aligned} \tag{3}$$

where $\tilde{\Delta}_m = \bar{\Delta}_m + 2K|m_s|^2$ is the effective detuning between the magnon mode and the driving field with $\bar{\Delta}_m = \Delta_m + g_{\rm mb}Q_s$. The noise forces acting on the mechanical membrane are $\xi^{\rm in} = \xi^{\rm th} + \xi^{\rm ex}$, where $\xi^{\rm th}$ and $\xi^{\rm ex}$ are the scaled thermal force and the detected force with dimension $\rm Hz^{1/2}$, respectively. All noise operators have zero mean: $\langle a^{\rm in}\rangle = \langle m^{\rm in}\rangle = \langle \xi^{\rm in}\rangle = 0$.

Considering a strong microwave drive field applied to directly pump the YIG sphere, thus we can expand each operator as the sum of its classical mean value and a small quantum fluctuation [58], i.e., $\hat{a} = a_s + \delta\hat{a}$, $\hat{Q} = Q_s + \delta\hat{Q}$, and $\hat{P} = P_s + \delta\hat{P}$, with $\langle\delta\hat{a}\rangle = \langle\delta\hat{Q}\rangle =$

$\langle\delta\hat{P}\rangle = 0$. By defining the quadrature fluctuation operators $\delta X_a = \left(\delta a + \delta a^\dagger\right)/\sqrt{2}, \delta X_m = \left(\delta m + \delta m^\dagger\right)/\sqrt{2}, \delta Y_a = \left(\delta a - \delta a^\dagger\right)/\sqrt{2}i, \delta Y_m = \left(\delta m - \delta m^\dagger\right)/\sqrt{2}i$ with the associated input noise operators $(\delta X_k^{\rm in}, \delta Y_k^{\rm in})(k = a, m)$ and corresponding correlation functions

$$\begin{aligned}
&\left\langle \delta X_{a(m)}^{\rm in}[\omega]\delta X_{a(m)}^{\rm in}[\omega']\right\rangle = \frac{1}{2}\delta(\omega+\omega'),\\
&\left\langle \delta Y_{a(m)}^{\rm in}[\omega]\delta Y_{a(m)}^{\rm in}[\omega']\right\rangle = \frac{1}{2}\delta(\omega+\omega'),\\
&\left\langle \delta X_{a(m)}^{\rm in}[\omega]\delta Y_{a(m)}^{\rm in}[\omega']\right\rangle = \frac{i}{2}\delta(\omega+\omega'),\\
&\left\langle \delta Y_{a(m)}^{\rm in}[\omega]\delta X_{a(m)}^{\rm in}[\omega']\right\rangle = -\frac{i}{2}\delta(\omega+\omega'),\\
&\left\langle \delta\xi^{\rm th}[\omega]\delta\xi^{\rm th}[\omega']\right\rangle = \bar{n}_m^T\delta(\omega+\omega'),
\end{aligned} \tag{4}$$

where $\bar{n}_m^T \approx \hbar\omega_m/k_{\rm B}T$, $k_{\rm B}$ is Boltzmann's constant, and T is the bath temperature. Then the linearized quantum Langevin equations describing the quadrature fluctuations $(\delta X_a, \delta Y_a, \delta X_m, \delta Y_m, \delta Q, \delta P)$ are given by

$$\begin{aligned}
\delta\dot{X}_a &= -\frac{\kappa_a}{2}\delta X_a + \Delta_c\delta Y_a + g_{\rm ma}\delta Y_m + \sqrt{\kappa_a}\delta X_a^{\rm in},\\
\delta\dot{Y}_a &= -\Delta_c\delta X_a - \frac{\kappa_m}{2}\delta Y_a - g_{\rm ma}\delta X_m + \sqrt{\kappa_a}\delta Y_a^{\rm in},\\
\delta\dot{X}_m &= -\frac{\kappa_m}{2}\delta X_m + \tilde{\Delta}_m\delta Y_m + g_{\rm ma}\delta Y_a - G\delta Q + \sqrt{\kappa_m}\delta X_m^{\rm in},\\
\delta\dot{Y}_m &= -\tilde{\Delta}_m\delta X_m - \frac{\kappa_m}{2}\delta Y_m - g_{\rm ma}\delta X_a + \sqrt{\kappa_m}\delta Y_m^{\rm in},\\
\delta\dot{Q} &= \omega_m\delta P,\quad \delta\dot{P} = G\delta Y_m - \omega_m\delta Q - \gamma_b\delta P + \xi^{\rm in}.
\end{aligned} \tag{5}$$

The effective magnomechanical coupling strength, $G = i\sqrt{2}g_{\rm mb}m_s$, can be adjusted by varying the strength of the drive field, Ω, which in turn modulates the magnomechanical cooperativity, $C = G^2/(\kappa_m\gamma_b)$. We also note that by changing the position of the loop antenna above the YIG sphere, the dissipation of the magnon mode (and consequently the magnomechanical cooperativity, C) is controlled [59].

We use a flow chart to depict the flow of backaction noise, as shown in Figure 2. For a conventional CMM system, magnons impart a radiation-pressure-like force on the phonons due to magnetostrictive interaction, introducing the magnomechanical backaction noise (Channel 1, red arrows in Figure 2). In the presence of the magnon Kerr effect, a direct coupling between magnon quadratures emerges, introducing a magnon-induced backaction noise path (Channel 2, blue arrow) [8]. As Figure 2 shows, the destructive interference between the two channels suppresses the backaction noise of the CMM sensor and thus enhances the sensitivity of the force sensing.

In practice, one often measures the field that escapes from the cavity to extract information about the intracavity field, because directly measuring the intracavity field is typically challenging. Thus, with the help of the input-output relation

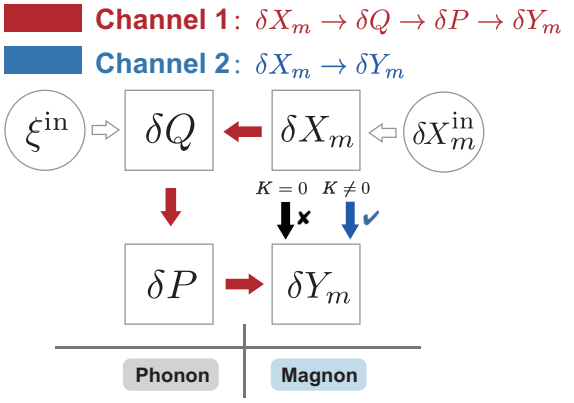

Figure 2 (Color online) Flow chart of dynamical backaction noise. Channel 1 (red arrows) represents the original magnomechanical backaction noise due to magnetostrictive interaction. Another path (blue arrow) can be introduced by utilizing the magnon Kerr effect. The destructive interference between Channel 1 and Channel 2 can reduce the impacts of the backaction noise and thus enhance the sensitivity of the force sensing.

Table 1 Experimentally accessible parameters

Parameter	Symbol	Value
Cavity mode frequency	ω_a	$2\pi\times 10$ GHz
Mechanical frequency	ω_b	$2\pi\times 10$ MHz
Cavity dissipation rate	κ_a	$2\pi\times 2$ MHz
Magnon dissipation rate	κ_m	$2\pi\times 2$ MHz
Mechanical damping rate	γ_b	$2\pi\times 10^2$ Hz
Amplitude of the magnetic field	B_0	3.9×10^{-5} T

$\delta a^{\rm out} = \sqrt{\kappa_a}\delta a - \delta a^{\rm in}$, one can read out the frequency-dependent force noise via homodyne detection. The output field is mixed with a reference field (i.e., a local oscillator with phase ϕ) at a 50:50 beam splitter. Then the measured quadrature is given by:

$$\delta X_{\phi,a}^{\rm out}[\omega] = \delta X_a^{\rm out}[\omega]\cos\phi + \delta Y_a^{\rm out}[\omega]\sin\phi. \tag{6}$$

The spectrum of the output field thus consists of amplitude or phase vacuum noise, thermal occupations, and quantum correlations (see Appendix for more details on definitions and calculations)

$$\begin{aligned}
\bar{S}_{\rm II}[\omega] &= \frac{1}{2}\left\langle\left\{\delta X_{\phi,a}^{\rm out}[\omega], \delta X_{\phi,a}^{\rm out}[-\omega]\right\}\right\rangle\\
&= \mathcal{R}_m^{\phi}\left(\bar{n}_m + \bar{n}_{\rm add}[\omega]\right),
\end{aligned} \tag{7}$$

where $\mathcal{R}_m^{\phi}$ is the mechanical response of our CMM sensor to the detected external force.

Here, the added noise $\bar{n}_{\rm add}$ includes both imprecision noise and quantum backaction noise, contributing to the total force noise spectrum, which is essential for quantifying the sensitivity of the force measurement

$$\bar{S}_{\rm FF}[\omega] = 2\hbar m_{\rm eff}\kappa_m\omega_b(\bar{n}_m^T + \bar{n}_{\rm add}[\omega]). \tag{8}$$

In the following, we subtract the contributions of thermal noise to reveal the influence of the magnon squeezing on the quantum noise and the performance of the CMM sensor.

Quantum squeezing is known to be capable of increasing the sensitivity of quantum sensors [12, 50, 57, 60-64]. In a CMM system, magnon quadratures can be indirectly correlated through the mechanical mode via the magnetostrictive interaction [54], resulting in a quadrature squeezing of the phonon [55, 56, 65, 66] and the magnon mode [18]. The magnon squeezing can also be achieved by utilizing the magnon Kerr nonlinearity. As detailed in ref. [18], the squeezing of the magnon mode can be transferred to the microwave cavity field [67-70], and the squeezing can be observed in the cavity output field via a homodyne detection. With identical parameters, the added noise is limited by the SQL for the non-squeezing case, while it can be suppressed below the SQL by tuning the magnon Kerr strength K.

As shown in Figure 3(a), the scaled added noise $\bar{n}_{\rm add}/\bar{n}_{\rm add}^{\rm SQL}$ is plotted for magnomechanical cooperativity C, with different magnon Kerr strength K. For $K = 0$ (i.e., in the absence of the magnon Kerr effect), there is always $\bar{n}_{\rm add}/\bar{n}_{\rm add}^{\rm SQL} > 1$, in sharp contrast to the situation when $K > 0$, for which $\bar{n}_{\rm add}/\bar{n}_{\rm add}^{\rm SQL}$ first decreases below 1 (i.e., beating the SQL, the best sensitivity existing in the absence of quantum correlations, represented by the gray line in the Figure 3(a)) with $C/C_{\rm SQL}$, and then increases with increasing $C/C_{\rm SQL}$ after reaching a minimum value. For $K/2\pi = 1.2$ nHz, the added quantum noise can be suppressed by up to two orders of magnitude below the SQL, and thus significantly enhancing the force sensing.

To determine the parameters corresponding to the minimum noise, we plot $\bar{n}_{\rm add}/\bar{n}_{\rm add}^{\rm SQL}$ as a function of the magnomechanical cooperativity C and magnon Kerr strength K, or the magnon-phonon coupling strength $g_{\rm mb}$ and the magnon-

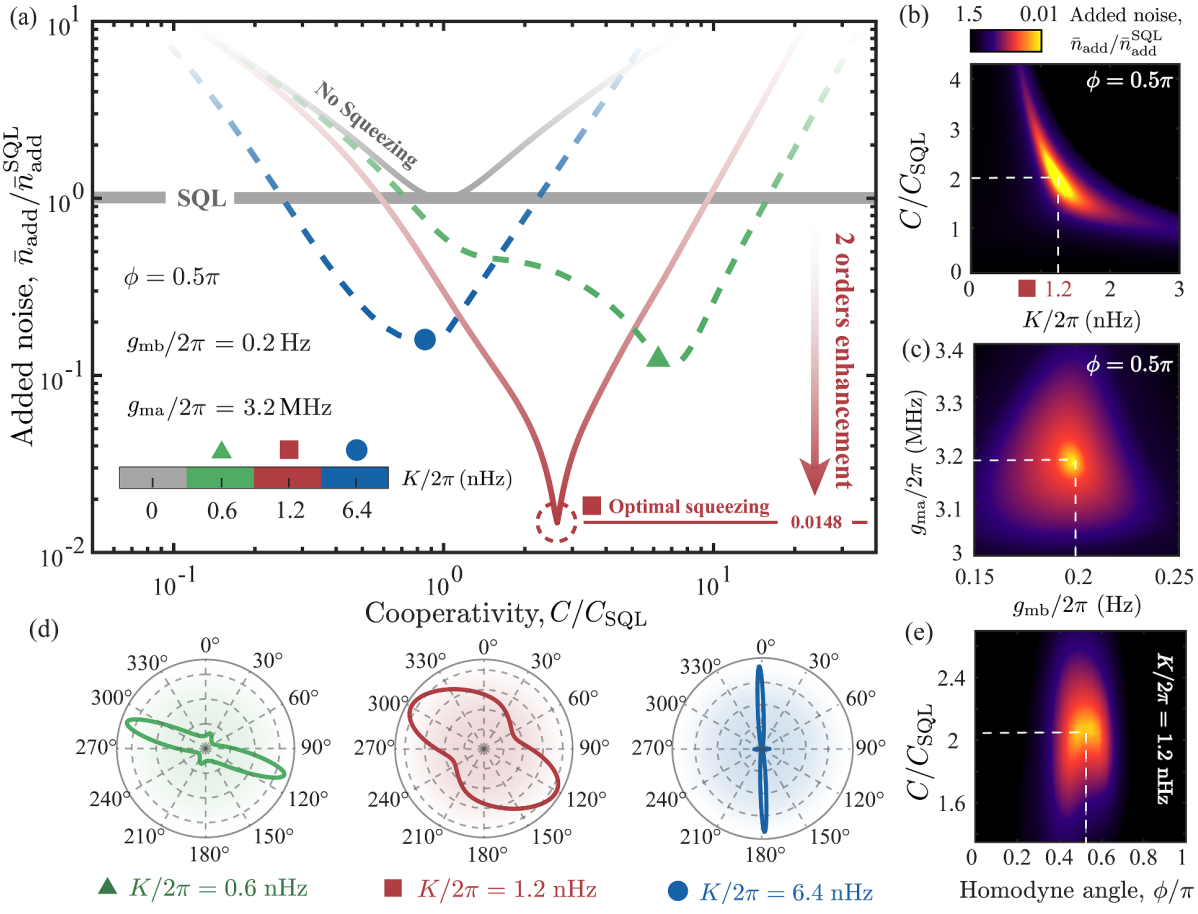

Figure 3 (Color online) (a) Weak force measurement below the standard quantum limit. Added noise (log scale) is plotted as a function of the cooperativity $C/C_{\rm SQL}$ with different magnon Kerr strengths K for the standard phase detection. The gray solid line corresponds to the SQL. The magnon-photon coupling strength $g_{\rm ma}/2\pi = 3.2$ MHz, and magnomechanical coupling strength $g_{\rm mb}/2\pi = 0.2$ Hz. (b) Quantum noise below the SQL, with suitable magnon Kerr strength K and magnomechanical cooperativity $C/C_{\rm SQL}$. (c) The scaled added noise $\bar{n}_{\rm add}/\bar{n}_{\rm add}^{\rm SQL}$ versus the magnomechanical coupling strength $g_{\rm mb}$ and the magnon-photon coupling strength $g_{\rm ma}$. (d) Added noise $\bar{n}_{\rm add}/\bar{n}_{\rm add}^{\rm SQL}$ versus the homodyne angle ϕ, when $K/2\pi = 0.6$, 1.2 and 6.4 nHz. (e) Density plot of the scaled added noise as a function of the cooperativity $C/C_{\rm SQL}$ and the homodyne angle ϕ. The parameters used for our numerical calculations are experimentally accessible and stable (see Table 1).

photon coupling strength g_{ma} in Figure 3(b) and (c). We find that the minimum added noise occurs for $C/C_{\mathrm{SQL}} = 2$, $K/2\pi = 1.2$ nHz, $g_{\mathrm{mb}}/2\pi = 0.2$ Hz, and $g_{\mathrm{ma}}/2\pi = 3.2$ MHz. Moreover, the two orders of magnitude improvement in sensitivity, compared to the result in the absence of magnon squeezing, as depicted in Figure 3(a), can be further enhanced by optimizing the homodyne detection (see Figure 3(d) and (e)). Physically, these phenomena can be understood by the generation of magnon squeezing, which can be facilitated by the destructive interference between the two channels of the backaction noise (see the discussion of Figure 2).

3 Conclusion and outlook

A distinct feature of our system lies in its intrinsic Kerr-type nonlinearities, which induce the magnon squeezing, thereby enhancing quantum force sensing, ground-state cooling, and quantum entanglement. Besides, the CMM systems exhibit remarkable experimental tunability compared to the COM systems, as the magnon frequency can be conveniently adjusted by the bias magnetic field. Furthermore, the ability to preserve good quantum coherence even at room temperature also provides an excellent opportunity to study coherent information processing [7, 30, 71], explore nonlinear properties of the CMM systems [24, 29-31], and take advantage of its broad compatibility with various quantum systems [4, 10], making it possible to further study coherent interactions between different systems.

In summary, we study the impact of quantum squeezing induced by the quantum correlations between the magnon quadratures on quantum-enhanced weak force sensing. We show that the performance of the CMM sensors can be significantly enhanced with considerably suppressed added quantum noise, achieving two orders of magnitude less noisy (that is, much more sensitive) than the SQL. Furthermore, we also show the impact of the homodyne angle, magnon-phonon coupling strength and magnon-photon coupling strength on the sensitivity of our CMM system. Our work not only reveals the significant impact of the magnon squeezing in the realm of quantum precision measurements, but also confirms that compact CMM systems can serve as powerful new tools for quantum sensing. Moreover, our results may potentially lead to the use of CMM systems in phonon laser to EP-enhanced quantum sensing [72-75]. We expect that such tools can play unique roles in applications involving magnetic signals such as seismics, geomagnetically-matching navigation, and biomedical diagnosis.

Hui Jing is supported by the National Natural Science Foundation of China (Grant No. 11935006), the Science and Technology Innovation Program of Hunan Province (Grant No. 2020RC4047), National Key R&D Program of China (Grant No. 2024YFE0102400) and Hunan Provincial Major Sci-tech Program (Grant No. 2023ZJ1010). Tian-Xiang Lu is supported by the National Natural Science Foundation of China (Grant No. 12205054), and Ph.D. Research Foundation (BSJJ202122). Ran Huang is supported by the Japan Society for the Promotion of Science (JSPS) Postdoctoral Fellowships for Research in Japan (No. P22018). Franco Nori is supported in part by: Nippon Telegraph and Telephone Corporation (NTT) Research, the Japan Science and Technology Agency (JST) (via the Quantum Leap Flagship Program (Q-LEAP), and the Moonshot R&D (Grant No. JPMJMS2061)), the Asian Office of Aerospace Research and Development (AOARD) (Grant No. FA2386-20-1-4069), and the Office of Naval Research (ONR) Global (Grant No. N62909-23-1-2074).

Conflict of interest The authors declare that they have no conflict of interest.

1 Y. Tabuchi, S. Ishino, T. Ishikawa, R. Yamazaki, K. Usami, and Y. Nakamura, Phys. Rev. Lett. **113**, 083603 (2014).
2 R. Hisatomi, A. Osada, Y. Tabuchi, T. Ishikawa, A. Noguchi, R. Yamazaki, K. Usami, and Y. Nakamura, Phys. Rev. B **93**, 174427 (2016).
3 D. Lachance-Quirion, Y. Tabuchi, S. Ishino, A. Noguchi, T. Ishikawa, R. Yamazaki, and Y. Nakamura, Sci. Adv. **3**, e1603150 (2017).
4 D. Lachance-Quirion, Y. Tabuchi, A. Gloppe, K. Usami, and Y. Nakamura, Appl. Phys. Express **12**, 070101 (2019).
5 S. P. Wolski, D. Lachance-Quirion, Y. Tabuchi, S. Kono, A. Noguchi, K. Usami, and Y. Nakamura, Phys. Rev. Lett. **125**, 17701 (2020).
6 B. Z. Rameshti, S. V. Kusminskiy, J. A. Haigh, K. Usami, D. Lachance-Quirion, Y. Nakamura, C.-M. Hu, H. X. Tang, G. E. W. Bauer, and Y. M. Blanter, Phys. Rep. **979**, 1 (2022).
7 X. Zhang, C. L. Zou, L. Jiang, and H. X. Tang, Phys. Rev. Lett. **113**, 156401 (2014).
8 C. A. Potts, Phys. Rev. X **12**, 070101 (2021).
9 X. Zuo, Z. Y. Fan, H. Qian, M. S. Ding, H. Tan, H. Xiong, and J. Li, New J. Phys. **26**, 031201 (2024).
10 X. Zhang, C. L. Zou, L. Jiang, and H. X. Tang, Sci. Adv. **2**, e1501286 (2016).
11 J. Li, S. Y. Zhu, and G. S. Agarwal, Phys. Rev. Lett. **121**, 203601 (2018).
12 H. Yu, L. McCuller, M. Tse, N. Kijbunchoo, L. Barsotti, N. Mavalvala, J. Betzwieser, C. D. Blair, S. E. Dwyer, A. Effler, M. Evans, A. Fernandez-Galiana, P. Fritschel, V. V. Frolov, F. Matichard, D. E. McClelland, T. McRae, A. Mullavey, D. Sigg, B. J. J. Slagmolen, C. Whittle, A. Buikema, Y. Chen, T. R. Corbitt, R. Schnabel, R. Abbott, C. Adams, R. X. Adhikari, A. Ananyeva, S. Appert, K. Arai, J. S. Areeda, Y. Asali, S. M. Aston, C. Austin, A. M. Baer, M. Ball, S. W. Ballmer, S. Banagiri, D. Barker, J. Bartlett, B. K. Berger, D. Bhattacharjee, G. Billingsley, S. Biscans, R. M. Blair, N. Bode, P. Booker, R. Bork, A. Bramley, A. F. Brooks, D. D. Brown, C. Cahillane, K. C. Cannon, X. Chen, A. A. Ciobanu, F. Clara, S. J. Cooper, K. R. Corley, S. T. Countryman, P. B. Covas, D. C. Coyne, L. E. H. Datrier, D. Davis, C. Di Fronzo, K. L. Dooley, J. C. Driggers, P. Dupej, T. Etzel, T. M. Evans, J. Feicht, P. Fulda, M. Fyffe, J. A. Giaime, K. D. Giardina, P. Godwin, E. Goetz, S. Gras, C. Gray, R. Gray, A. C. Green, A. Gupta, E. K. Gustafson, R. Gustafson, J. Hanks, J. Hanson, T. Hardwick, R. K. Hasskew, M. C. Heintze, A. F. Helmling-Cornell, N. A. Holland, J. D. Jones, S. Kandhasamy, S. Karki, M. Kasprzack, K. Kawabe, P. J. King, J. S. Kissel, R. Kumar, M. Landry, B. B. Lane, B. Lantz, M. Laxen, Y. K. Lecoeuche, J. Leviton, J. Liu, M. Lormand, A. P. Lundgren, R. Macas, M. MacInnis, D. M. Macleod, G. L. Mansell, S. Márka, Z. Márka, D. V. Martynov, K. Mason, T. J. Massinger, R. McCarthy, S. McCormick, J. McIver, G. Mendell, K. Merfeld, E. L. Merilh, F. Meylahn, T. Mistry, R. Mittleman, G. Moreno, C. M. Mow-Lowry, S. Mozzon, T. J. N. Nelson, P. Nguyen, L. K. Nuttall, J. Oberling, R. J. Oram, C. Osthelder, D. J. Ottaway, H. Overmier, J. R. Palamos, W. Parker, E. Payne, A. Pele, C. J. Perez, M. Pirello, H. Radkins, K. E.

Ramirez, J. W. Richardson, K. Riles, N. A. Robertson, J. G. Rollins, C. L. Romel, J. H. Romie, M. P. Ross, K. Ryan, T. Sadecki, E. J. Sanchez, L. E. Sanchez, T. R. Saravanan, R. L. Savage, D. Schaetzl, R. M. S. Schofield, E. Schwartz, D. Sellers, T. Shaffer, J. R. Smith, S. Soni, B. Sorazu, A. P. Spencer, K. A. Strain, L. Sun, M. J. Szczepańczyk, M. Thomas, P. Thomas, K. A. Thorne, K. Toland, C. I. Torrie, G. Traylor, A. L. Urban, G. Vajente, G. Valdes, D. C. Vander-Hyde, P. J. Veitch, K. Venkateswara, G. Venugopalan, A. D. Viets, T. Vo, C. Vorvick, M. Wade, R. L. Ward, J. Warner, B. Weaver, R. Weiss, B. Willke, C. C. Wipf, L. Xiao, H. Yamamoto, H. Yu, L. Zhang, M. E. Zucker, and J. Zweizig, Nature **583**, 43 (2020).

13 Z. Fan, L. Qiu, S. Gröblacher, and J. Li, Laser Photonics Rev. **17**, 2200866 (2023).

14 Z. Y. Fan, H. Qian, X. Zuo, and J. Li, Phys. Rev. A **108**, 023501 (2023).

15 D. Xu, X. K. Gu, H. K. Li, Y. C. Weng, Y. P. Wang, J. Li, H. Wang, S. Y. Zhu, and J. Q. You, Phys. Rev. Lett. **130**, 193603 (2023).

16 Y. Wang, W. Xiong, Z. Xu, G.-Q. Zhang, and J.-Q. You, Sci. China-Phys. Mech. Astron. **65**, 260314 (2021).

17 J. Li, and S. Y. Zhu, New J. Phys. **21**, 085001 (2019).

18 J. Li, Y.-P. Wang, J.-Q. You, and S.-Y. Zhu, Nat. Sci. Rev. **10**, nwac247 (2023).

19 J. Li, and S. Gröblacher, Quantum Sci. Technol. **6**, 024005 (2021).

20 G. T. Xu, M. Zhang, Y. Wang, Z. Shen, G. C. Guo, and C. H. Dong, Phys. Rev. Lett. **131**, 243601 (2023).

21 Y. Wang, H.-L. Zhang, J.-L. Wu, J. Song, K. Yang, W. Qin, H. Jing, and L.-M. Kuang, Sci. China-Phys. Mech. Astron. **66**, 110311 (2023).

22 A. Kani, B. Sarma, and J. Twamley, Phys. Rev. Lett. **128**, 013602 (2022).

23 J. Qian, J. Li, S.-Y. Zhu, J. Q. You, and Y.-P. Wang, arXiv:2307.03944

24 Y. P. Wang, G. Q. Zhang, D. Zhang, X. Q. Luo, W. Xiong, S. P. Wang, T. F. Li, C. M. Hu, and J. Q. You, Phys. Rev. B **94**, 224410 (2016).

25 M. Scully, and M. Zubairy, Quantum Optics, (Cambridge University Press, Cambridge, 1996).

26 G. S. Agarwal, Quantum optics (Cambridge University Press, Cambridge, 2013).

27 Z. Zhang, M. O. Scully, and G. S. Agarwal, Phys. Rev. Res. **1**, 023021 (2019).

28 Z. B. Yang, W. J. Wu, J. Li, Y. P. Wang, and J. Q. You, Phys. Rev. A **106**, 012419 (2022).

29 G. Q. Zhang, Y. P. Wang, and J. Q. You, Sci. China-Phys. Mech. Astron. **62**, 987511 (2019).

30 Y. P. Wang, G. Q. Zhang, D. Zhang, T. F. Li, C. M. Hu, and J. Q. You, Phys. Rev. Lett. **120**, 057202 (2018).

31 R. C. Shen, Y. P. Wang, J. Li, S. Y. Zhu, G. S. Agarwal, and J. Q. You, Phys. Rev. Lett. **127**, 183202 (2021).

32 R.-C. Shen, J. Li, Z.-Y. Fan, Y.-P. Wang, and J. Q. You, Phys. Rev. Lett. **129**, 123601 (2022).

33 M. Asjad, J. Li, S.-Y. Zhu, and J. Q. You, Fundam. Res. **3**, 3 (2022).

34 D. Zoepfl, M. L. Juan, N. Diaz-Naufal, C. M. F. Schneider, L. F. Deeg, A. Sharafiev, A. Metelmann, and G. Kirchmair, Phys. Rev. Lett. **130**, 033601 (2023).

35 Q. Zheng, W. Zhong, G. Cheng, and A. Chen, Optics Commun. **546**, 129796 (2023).

36 C. Kong, J. Liu, and H. Xiong, Front. Phys. **18**, 12501 (2023).

37 C. Kong, H. Xiong, and Y. Wu, Phys. Rev. Appl. **12**, 034001 (2019).

38 D. Mason, J. Chen, M. Rossi, Y. Tsaturyan, and A. Schliesser, Nat. Phys. **15**, 745 (2019).

39 W. Zhao, S.-D. Zhang, A. Miranowicz, and H. Jing, Sci. China-Phys. Mech. Astron. **63**, 224211 (2019).

40 T. Gebremariam, Y.-X. Zeng, M. Mazaheri , and C. Li, Sci. China-Phys. Mech. Astron. **63**, 210311 (2020).

41 Y.-W. Hu, Y.-F. Xiao, Y.-C. Liu, and Q. Gong, Front. Phys. **8**, 475 (2013).

42 S. Forstner, S. Prams, J. Knittel, E. D. van Ooijen, J. D. Swaim, G. I. Harris, A. Szorkovszky, W. P. Bowen, and H. Rubinsztein-Dunlop, Phys. Rev. Lett. **108**, 120801 (2012).

43 S. Forstner, E. Sheridan, J. Knittel, C. L. Humphreys, G. A. Brawley, H. Rubinsztein-Dunlop, and W. P. Bowen, Adv. Mater. **26**, 6348 (2014).

44 F. Gotardo, B. J. Carey, H. Greenall, G. I. Harris, E. Romero, D. Bulla, E. M. Bridge, J. S. Bennett, S. Foster, and W. P. Bowen, Opt. Express **31**, 37663 (2023).

45 A. G. Krause, M. Winger, T. D. Blasius, Q. Lin, and O. Painter, Nat. Photon. **6**, 768 (2012).

46 F. G. Cervantes, L. Kumanchik, J. Pratt, and J. M. Taylor, Appl. Phys. Lett. **104**, 221111 (2014).

47 M. Koppenhöfer, C. Padgett, J. V. Cady, V. Dharod, H. Oh, A. C. Bleszynski Jayich, and A. A. Clerk, Phys. Rev. Lett. **130**, 093603 (2023).

48 W. Yu, W. C. Jiang, Q. Lin, and T. Lu, Nat. Commun. **7**, 12311 (2016).

49 M. Sansa, M. Defoort, A. Brenac, M. Hermouet, L. Banniard, A. Fafin, M. Gely, C. Masselon, I. Favero, G. Jourdan, and S. Hentz, Nat. Commun. **11**, 3781 (2020).

50 Y. Xia, A. R. Agrawal, C. M. Pluchar, A. J. Brady, Z. Liu, Q. Zhuang, D. J. Wilson, and Z. Zhang, Nat. Photon. **17**, 470 (2023).

51 Z. Shen, G. T. Xu, M. Zhang, Y. L. Zhang, Y. Wang, C. Z. Chai, C. L. Zou, G. C. Guo, and C. H. Dong, Phys. Rev. Lett. **129**, 243601 (2022).

52 T. Chalopin, C. Bouazza, A. Evrard, V. Makhalov, D. Dreon, J. Dalibard, L. A. Sidorenkov, and S. Nascimbene, Nat. Commun. **9**, 4955 (2018).

53 B. J. Lawrie, P. D. Lett, A. M. Marino, and R. C. Pooser, ACS Photonics **6**, 1307 (2019).

54 F. Nori, R. Merlin, S. Haas, A. W. Sandvik, and E. Dagotto, Phys. Rev. Lett. **75**, 553 (1995).

55 X. Hu, and F. Nori, Phys. Rev. Lett. **76**, 2294 (1996).

56 X. Hu, and F. Nori, Phys. Rev. Lett. **79**, 4605 (1997).

57 G. Y. Xiang, B. L. Higgins, D. W. Berry, H. M. Wiseman, and G. J. Pryde, Nat. Photon. **5**, 43 (2010).

58 M. Aspelmeyer, T. J. Kippenberg, and F. Marquardt, Rev. Mod. Phys. **86**, 1391 (2014).

59 Y. Yang, Y.-P. Wang, J. W. Rao, Y. S. Gui, B. M. Yao, W. Lu, and C.-M. Hu, Phys. Rev. Lett. **125**, 147202 (2020).

60 F. Martin Ciurana, G. Colangelo, L. Slodička, R. J. Sewell, and M. W. Mitchell, Phys. Rev. Lett. **119**, 043603 (2017).

61 L. Z. Liu, Y. Z. Zhang, Z. D. Li, R. Zhang, X. F. Yin, Y. Y. Fei, L. Li, N. L. Liu, F. Xu, Y. A. Chen, and J. W. Pan, Nat. Photon. **15**, 137 (2021).

62 J.-X. Liu, Y.-F. Jiao, Y. Li, X.-W. Xu, Q.-Y. He, and H. Jing, Sci. China-Phys. Mech. Astron. **66**, 230312 (2023).

63 A. J. Brady, X. Chen, Y. Xia, J. Manley, M. Dey Chowdhury, K. Xiao, Z. Liu, R. Harnik, D. J. Wilson, Z. Zhang, and Q. Zhuang, Commun Phys **6**, 1 (2023).

64 J. Ma, X. Wang, C.-P. Sun, and F. Nori, Phys. Rep. **509**, 89 (2011).

65 X. Hu, and F. Nori, Phys. Rev. B **53**, 2419 (1996).

66 X. Hu, and F. Nori, Physica B: Condensed Matter **263**, 16 (1999).

67 A. M. Zagoskin, E. Il'chev, M. W. McCutcheon, J. F. Young, and F. Nori, Phys. Rev. Lett. **101**, 253602 (2008).

68 A. M. Zagoskin, E. Il'ichev, and F. Nori, Phys. Rev. A **85**, 063811 (2012).

69 L. Tang, J. Tang, M. Chen, F. Nori, M. Xiao, and K. Xia, Phys. Rev. Lett. **128**, 083604 (2022).

70 W. Qin, A. Miranowicz, and F. Nori, Phys. Rev. Lett. **129**, 123602 (2022).

71 D. Zhang, X.-M. Wang, T.-F. Li, X.-Q. Luo, W. Wu, F. Nori, and J. Q. You, npj Quantum Inf. **1**, 15014 (2015).

72 H. Jing, K. Özdemir, X. Y. Lü, J. Zhang, L. Yang, and F. Nori, Phys. Rev. Lett. **113**, 053604 (2014).

73 T.-X. Lu, Y. Wang, K. Xia, X. Xiao, L.-M. Kuang, and H. Jing, Sci. China-Phys. Mech. Astron. **67**, 260312 (2024).

74 T. Kuang, R. Huang, W. Xiong, Y. Zuo, X. Han, F. Nori, C.-W. Qiu, H. Luo, H. Jing, and G. Xiao, Nat. Phys. **19**, 414 (2023).

75 X.-W. Xu, J.-Q. Liao, H. Jing, and L.-M. Kuang, Sci. China-Phys. Mech. Astron. **66**, 100312 (2023).

Appendix

A1 Derivation of the added quantum noise

The output fluctuations in the amplitude and phase quadratures of the cavity and magnon modes to be measured in the Fourier domain can be derived from

$$\begin{pmatrix}\delta X_a^{out}\\ \delta Y_a^{out}\\ \delta X_m^{out}\\ \delta Y_m^{out}\end{pmatrix}=\begin{pmatrix}\mathcal{A}_a & \mathcal{B}_a & \mathcal{C}_a & \mathcal{D}_a & \mathcal{E}_a\\ \mathcal{F}_a & \mathcal{G}_a & \mathcal{H}_a & \mathcal{I}_a & \mathcal{J}_a\\ \mathcal{A}_m & \mathcal{B}_m & \mathcal{C}_m & \mathcal{D}_m & \mathcal{E}_m\\ \mathcal{F}_m & \mathcal{G}_m & \mathcal{H}_m & \mathcal{I}_m & \mathcal{J}_m\end{pmatrix}\times\left(\delta X_a^{\rm in}\ \delta Y_a^{\rm in}\ \delta X_m^{\rm in}\ \delta Y_m^{\rm in}\ \delta\xi^{\rm in}\right)^{\rm T},\tag{a1}$$

where

$$\begin{aligned}\mathcal{A}_a&=\sqrt{\kappa_a}\mathrm{A}_1-1, & \mathcal{F}_a&=\sqrt{\kappa_a}\mathrm{A}_3,\\ \mathcal{B}_a&=\sqrt{\kappa_a}\mathrm{B}_1, & \mathcal{G}_a&=\sqrt{\kappa_a}\mathrm{B}_3-1,\\ \mathcal{C}_a&=\sqrt{\kappa_a}\mathrm{C}_1, & \mathcal{H}_a&=\sqrt{\kappa_a}\mathrm{C}_3,\\ \mathcal{D}_a&=\sqrt{\kappa_a}\mathrm{D}_1, & \mathcal{I}_a&=\sqrt{\kappa_a}\mathrm{D}_3,\\ \mathcal{E}_a&=\sqrt{\kappa_a}\mathrm{E}_1, & J_a&=\sqrt{\kappa_a}\mathrm{E}_3,\end{aligned}\tag{a2}$$

$$\begin{aligned}\mathcal{A}_m&=\sqrt{\kappa_m}\mathrm{A}_2, & \mathcal{F}_m&=\sqrt{\kappa_m}\mathrm{A}_4,\\ \mathcal{B}_m&=\sqrt{\kappa_m}\mathrm{B}_2, & \mathcal{G}_m&=\sqrt{\kappa_m}\mathrm{B}_4,\\ \mathcal{C}_m&=\sqrt{\kappa_m}\mathrm{C}_2-1, & \mathcal{H}_m&=\sqrt{\kappa_m}\mathrm{C}_4,\\ \mathcal{D}_m&=\sqrt{\kappa_m}\mathrm{D}_2, & \mathcal{I}_m&=\sqrt{\kappa_m}\mathrm{D}_4-1,\\ \mathcal{E}_m&=\sqrt{\kappa_m}\mathrm{E}_2, & J_m&=\sqrt{\kappa_m}\mathrm{E}_4,\end{aligned}\tag{a3}$$

$$\begin{aligned}\mathrm{A}_1&=\frac{\mathcal{E}_+\mathcal{B}_-+\mathcal{C}_+\mathcal{A}_-}{\mathcal{A}_+\mathcal{A}_--\mathcal{B}_+\mathcal{B}_-}+\mu\left(\frac{\mathcal{A}_-\mathcal{H}_++\mathcal{B}_-\mathcal{H}_-}{\mathcal{A}_+\mathcal{A}_--\mathcal{B}_+\mathcal{B}_-}\right),\\ \mathrm{B}_1&=\frac{\mathcal{F}_-\mathcal{B}_-+\mathcal{D}_+\mathcal{A}_-}{\mathcal{A}_+\mathcal{A}_--\mathcal{B}_+\mathcal{B}_-}+\sigma\left(\frac{\mathcal{A}_-\mathcal{H}_++\mathcal{B}_-\mathcal{H}_-}{\mathcal{A}_+\mathcal{A}_--\mathcal{B}_+\mathcal{B}_-}\right),\\ \mathrm{C}_1&=\frac{\mathcal{E}_-\mathcal{A}_-+\mathcal{C}_-\mathcal{B}_-}{\mathcal{A}_+\mathcal{A}_--\mathcal{B}_+\mathcal{B}_-}+\rho\left(\frac{\mathcal{A}_-\mathcal{H}_++\mathcal{B}_-\mathcal{H}_-}{\mathcal{A}_+\mathcal{A}_--\mathcal{B}_+\mathcal{B}_-}\right),\\ \mathrm{D}_1&=\frac{\mathcal{F}_+\mathcal{A}_-+\mathcal{D}_-\mathcal{B}_-}{\mathcal{A}_+\mathcal{A}_--\mathcal{B}_+\mathcal{B}_-}+\nu\left(\frac{\mathcal{A}_-\mathcal{H}_++\mathcal{B}_-\mathcal{H}_-}{\mathcal{A}_+\mathcal{A}_--\mathcal{B}_+\mathcal{B}_-}\right),\end{aligned}\tag{a4}$$

$$\begin{aligned}\mathrm{A}_2&=\frac{\mathcal{E}_+\mathcal{A}_++\mathcal{C}_+\mathcal{B}_+}{\mathcal{A}_+\mathcal{A}_--\mathcal{B}_+\mathcal{B}_-}+\mu\left(\frac{\mathcal{A}_+\mathcal{H}_-+\mathcal{B}_+\mathcal{H}_+}{\mathcal{A}_+\mathcal{A}_--\mathcal{B}_+\mathcal{B}_-}\right),\\ \mathrm{B}_2&=\frac{\mathcal{F}_-\mathcal{A}_++\mathcal{D}_+\mathcal{B}_+}{\mathcal{A}_+\mathcal{A}_--\mathcal{B}_+\mathcal{B}_-}+\sigma\left(\frac{\mathcal{A}_+\mathcal{H}_-+\mathcal{B}_+\mathcal{H}_+}{\mathcal{A}_+\mathcal{A}_--\mathcal{B}_+\mathcal{B}_-}\right),\\ \mathrm{C}_2&=\frac{\mathcal{E}_-\mathcal{B}_++\mathcal{C}_-\mathcal{A}_+}{\mathcal{A}_+\mathcal{A}_--\mathcal{B}_+\mathcal{B}_-}+\rho\left(\frac{\mathcal{A}_+\mathcal{H}_-+\mathcal{B}_+\mathcal{H}_+}{\mathcal{A}_+\mathcal{A}_--\mathcal{B}_+\mathcal{B}_-}\right),\\ \mathrm{D}_2&=\frac{\mathcal{F}_+\mathcal{B}_++\mathcal{D}_-\mathcal{A}_+}{\mathcal{A}_+\mathcal{A}_--\mathcal{B}_+\mathcal{B}_-}+\nu\left(\frac{\mathcal{A}_+\mathcal{H}_-+\mathcal{B}_+\mathcal{H}_+}{\mathcal{A}_+\mathcal{A}_--\mathcal{B}_+\mathcal{B}_-}\right),\end{aligned}\tag{a5}$$

$$\begin{aligned}\mathrm{A}_3&=\Delta_a\Lambda_1\mathrm{A}_1-\Lambda_2\mathrm{A}_3+\sqrt{2}Q_a\mu-\sqrt{\kappa_a}\Delta_a\chi_0^2\chi_1\chi,\\ \mathrm{B}_3&=\Delta_a\Lambda_1\mathrm{B}_1-\Lambda_2\mathrm{B}_3+\sqrt{2}Q_a\sigma+\sqrt{\kappa_a}\chi_0\chi_1\chi,\\ \mathrm{C}_3&=\Delta_a\Lambda_1\mathrm{C}_1-\Lambda_2\mathrm{C}_3+\sqrt{2}Q_a\rho+\sqrt{\kappa_m}\Delta_a\tilde{\Delta}_m g_{\rm ma}\chi_0^4\chi_1^2\chi,\\ \mathrm{D}_3&=\Delta_a\Lambda_1\mathrm{D}_1-\Lambda_2\mathrm{D}_3+\sqrt{2}Q_a\nu-\sqrt{\kappa_m}\Delta_a g_{\rm ma}\chi_0^3\chi_1^2\chi,\\ \mathrm{A}_4&=\tilde{\Delta}_m\Lambda_1\mathrm{A}_3-\Lambda_2\mathrm{A}_1+\sqrt{2}Q_m\mu+\sqrt{\kappa_a}\Delta_a\tilde{\Delta}_m g_{\rm ma}\chi_0^4\chi_1^2\chi,\\ \mathrm{B}_4&=\tilde{\Delta}_m\Lambda_1\mathrm{B}_3-\Lambda_2\mathrm{B}_1+\sqrt{2}Q_m\sigma-\sqrt{\kappa_a}\tilde{\Delta}_m g_{\rm ma}\chi_0^3\chi_1^2\chi,\\ \mathrm{C}_4&=\tilde{\Delta}_m\Lambda_1\mathrm{C}_3-\Lambda_2\mathrm{C}_1+\sqrt{2}Q_m\rho-\sqrt{\kappa_a}\tilde{\Delta}_m\chi_0^2\chi_1\chi,\\ \mathrm{D}_4&=\tilde{\Delta}_m\Lambda_1\mathrm{D}_3-\Lambda_2\mathrm{D}_1+\sqrt{2}Q_m\nu+\sqrt{\kappa_a}\chi_0\chi_1\chi,\end{aligned}\tag{a6}$$

with

$$\begin{aligned}\chi_0&=\left(-i\omega+\frac{\gamma}{2}\right)^{-1},\\ \chi_m&=\omega_m\left(\omega_m^2-\omega^2-i\omega\Gamma_M\right)^{-1},\\ \chi_1&=\left(1+\Delta_a^2\chi_0^2\right)^{-1},\\ \Lambda_1&=g_{\rm ma}^2\chi_0^3\chi_1^2\chi,\\ \chi_2&=\left(1-G_m\chi_m\eta\right)^{-1},\\ \Lambda_2&=g_{\rm ma}\chi_0\chi_1\chi,\\ \chi_3&=\left(1-\Delta_a\tilde{\Delta}_m g_{\rm ma}^2\chi_0^4\chi_1^2\right)^{-1},\end{aligned}\tag{a7}$$

$$\begin{aligned}\eta=&\tilde{\Delta}_m g_{\rm ma}^2\chi_0^3\chi_1^2\chi\left(\frac{a_1q_m+a_2q_a}{a_1m_1-a_2m_2}\right)\\ &-g_{\rm ma}\chi_0\chi_1\chi\left(\frac{m_1q_a+m_2q_m}{a_1m_1-a_2m_2}\right)+\sqrt{2}Q_m,\\ \mu=&G\tilde{\Delta}_m\Lambda\chi_m\chi_2\left(\frac{\mathcal{E}_+\mathcal{A}_++\mathcal{C}_+\mathcal{B}_+}{\mathcal{A}_+\mathcal{A}_--\mathcal{B}_+\mathcal{B}_-}\right)\\ &-G\Lambda_2\chi_m\chi_2\left(\frac{\mathcal{E}_+\mathcal{B}_-+\mathcal{C}_+\mathcal{A}_-}{\mathcal{A}_+\mathcal{A}_--\mathcal{B}_+\mathcal{B}_-}\right)\\ &+\sqrt{\kappa_a}G\Delta_a\tilde{\Delta}_m g_{\rm ma}\chi_0^4\chi_1^2\chi\chi_m\chi_2,\\ \sigma=&G\tilde{\Delta}_m\Lambda\chi_m\chi_2\left(\frac{\mathcal{F}_-\mathcal{A}_++\mathcal{D}_+\mathcal{B}_+}{\mathcal{A}_+\mathcal{A}_--\mathcal{B}_+\mathcal{B}_-}\right)\\ &-G\Lambda_2\chi_m\chi_2\left(\frac{\mathcal{F}_-\mathcal{B}_-+\mathcal{D}_+\mathcal{A}_-}{\mathcal{A}_+\mathcal{A}_--\mathcal{B}_+\mathcal{B}_-}\right)\\ &-\sqrt{\kappa_a}G\tilde{\Delta}_m g_{\rm ma}\chi_0^3\chi_1^2\chi\chi_m\chi_2,\\ \rho=&G\tilde{\Delta}_m\Lambda\chi_m\chi_2\left(\frac{\mathcal{E}_-\mathcal{B}_++\mathcal{C}_-\mathcal{A}_+}{\mathcal{A}_+\mathcal{A}_--\mathcal{B}_+\mathcal{B}_-}\right)\\ &-G\Lambda_2\chi_m\chi_2\left(\frac{\mathcal{E}_-\mathcal{A}_-+\mathcal{C}_-\mathcal{B}_-}{\mathcal{A}_+\mathcal{A}_--\mathcal{B}_+\mathcal{B}_-}\right)\\ &-\sqrt{\kappa_m}G\tilde{\Delta}_m\chi_0^2\chi_1\chi\chi_m\chi_2,\\ \nu=&G\tilde{\Delta}_m\Lambda\chi_m\chi_2\left(\frac{\mathcal{F}_+\mathcal{B}_++\mathcal{D}_-\mathcal{A}_+}{\mathcal{A}_+\mathcal{A}_--\mathcal{B}_+\mathcal{B}_-}\right)\\ &-G\Lambda_2\chi_m\chi_2\left(\frac{\mathcal{F}_+\mathcal{A}_-+\mathcal{D}_-\mathcal{B}_-}{\mathcal{A}_+\mathcal{A}_--\mathcal{B}_+\mathcal{B}_-}\right)\\ &+\sqrt{\kappa_m}G\chi_0\chi_1\chi\chi_m\chi_2,\end{aligned}\tag{a8}$$

where

$$\begin{aligned}
\mathcal{A}_\pm &= 1-\Delta_\pm^2 g_{\rm ma}^2\chi_0^4\chi_1^2\chi+g_{\rm ma}^2\chi_0^2\chi_1\chi,\\
\mathcal{B}_\pm &= \Delta_\pm g_{\rm ma}^3\chi_0^4\chi_1^2\chi-\Delta_\mp g_{\rm ma}\chi_0^2\chi_1\chi,\\
\mathcal{C}_\pm &= \sqrt{\kappa_a}\chi_0+\sqrt{\kappa_a}\Delta_+\Delta_- g_{\rm ma}^2\chi_0^5\chi_1^2\chi-\sqrt{\kappa_a}\Delta_\pm^2\chi_0^3\chi_1\chi,\\
\mathcal{D}_\pm &= \sqrt{\kappa_a}\Delta_\pm\chi_0^2\chi_1\chi-\sqrt{\kappa_a}\Delta_\mp g_{\rm ma}^2\chi_0^4\chi_1^2\chi,\\
\mathcal{E}_\pm &= \sqrt{\kappa_a}\Delta_\mp^2\Delta_\pm g_{\rm ma}\chi_0^5\chi_1^2\chi-\sqrt{\kappa_a}\Delta_\pm g_{\rm ma}\chi_0^3\chi_1\chi,\\
\mathcal{F}_\pm &= \sqrt{\kappa_a}g_{\rm ma}\chi_0^2\chi_1\chi-\sqrt{\kappa_a}\Delta_\pm^2 g_{\rm ma}\chi_0^4\chi_1^2\chi,\\
\mathcal{G}_\pm &= \Delta_\pm g_{\rm ma}g_{\rm mb}m_s\chi_0^3\chi_1^2\chi,\\
\mathcal{H}_\pm &= \sqrt{2}Q_\pm\Delta_\pm\chi_0+\sqrt{2}Q_\mp g_{\rm ma}\chi_0.
\end{aligned}\tag{a9}$$

We measure the force noise by homodyne detection, in which the photocurrent I is proportional to the rotated field quadrature

$$\delta X_{\phi,a}^{\rm out}[\omega]=\delta X_a^{\rm out}[\omega]\cos\phi+\delta Y_a^{\rm out}[\omega]\sin\phi.\tag{a10}$$

In the Fourier domain, the quadratures of the output fields are given by

$$\begin{aligned}
\bar{S}_{\rm II}[\omega] &= \frac{1}{2}\left\langle\left\{\delta X_{\phi,a}^{\rm out}[\omega],\delta X_{\phi,a}^{\rm out}[-\Omega]\right\}\right\rangle\\
&= \mathcal{R}_m^\phi\left(\bar{n}_m+\bar{n}_{\rm add}[\omega]\right),
\end{aligned}\tag{a11}$$

where the mechanical response of the system to the detected force signal is derived as

$$\mathcal{R}_m^\phi = \mathcal{E}_a^2\cos^2\phi+\mathcal{J}_a^2\sin^2\phi+\mathcal{E}_a\mathcal{J}_a\sin(2\phi),\tag{a12}$$

and the added noise consisting of the imprecision noise and backaction noise is

$$\begin{aligned}
\bar{n}_{\rm add} =& \frac{1}{2}\left(\frac{\mathcal{A}_a^2+\mathcal{B}_a^2+\mathcal{C}_a^2+\mathcal{D}_a^2+i\mathcal{A}_a\mathcal{C}_a+i\mathcal{B}_a\mathcal{D}_a}{\mathcal{E}_a^2\cos^2\phi+\mathcal{J}_a^2\sin^2\phi+\mathcal{E}_a\mathcal{J}_a\sin(2\phi)}\right)\cos^2\phi\\
&+\frac{1}{2}\left(\frac{\mathcal{F}_a^2+\mathcal{G}_a^2+\mathcal{H}_a^2+\mathcal{I}_a^2+i\mathcal{F}_a\mathcal{H}_a+i\mathcal{G}_a\mathcal{I}_a}{\mathcal{E}_a^2\cos^2\phi+\mathcal{J}_a^2\sin^2\phi+\mathcal{E}_a\mathcal{J}_a\sin(2\phi)}\right)\sin^2\phi\\
&+\frac{1}{4}\left(\frac{\mathcal{A}_a\mathcal{F}_a+\mathcal{B}_a\mathcal{G}_a+\mathcal{C}_a\mathcal{H}_a+\mathcal{D}_a\mathcal{I}_a}{\mathcal{E}_a^2\cos^2\phi+\mathcal{J}_a^2\sin^2\phi+\mathcal{E}_a\mathcal{J}_a\sin(2\phi)}\right)\sin(2\phi).
\end{aligned}\tag{a13}$$

The sensitivity of the force measurement is typically characterized by the noise power spectral density (PSD)

$$\bar{S}_{\rm FF}[\omega]=2\hbar m_{\rm eff}\gamma_b\omega_b(\bar{n}_m^T+\bar{n}_{\rm add}).\tag{a14}$$

In Figure a1, similar features as in Figure 3(a) arise, noise suppressions and thus giant enhancement of the force sensitivities was achieved. Figure a1 shows that the PSD of the homodyne measurements shares the same dependency on the magnon Kerr strength K as the added quantum noise. Specifically, the PSD decreases as K increases, until reaching a minimum value and then increases, which is in agreement with the performance of the added quantum noise shown in Figure 3.

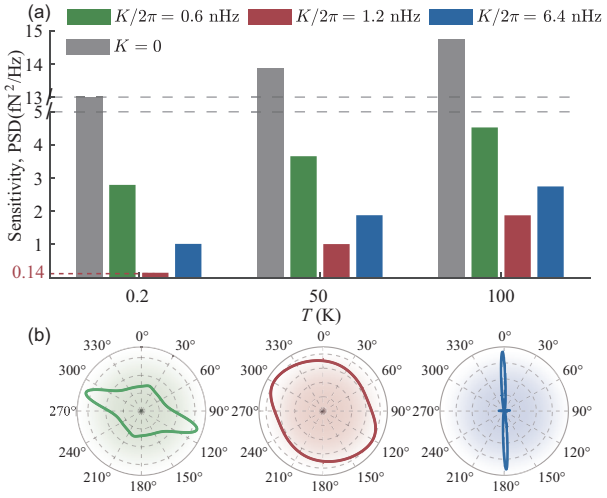

Figure a1 (Color online) Noise power spectral density (PSD) of homodyne measurements versus (a) the homodyne angle ϕ (b) the temperature when $K/2\pi$ = 0.6, 1.2, 6.4 nHz. The parameters are the same as those in Figure 3.

A2 Stability analysis

Finally, we analyze the stability properties of the CMM system by applying the Routh-Hurwitz criterion.

The characteristic equation of $|\mathrm{C}-\lambda\mathrm{I}|=0$ can be reduced to:

$$a_0\lambda^6+a_1\lambda^5+a_2\lambda^4+a_3\lambda^3+a_4\lambda^2+a_5\lambda^1+a_6=0,\tag{a15}$$

where $a_0=1$, $a_1=2\kappa_a+\gamma_b$ and

$$\begin{aligned}
a_2 =& \Delta_c^2+2g_{\rm ma}^2+\frac{3\kappa_a^2}{2}+2\kappa_a\gamma_b+\tilde{\Delta}_m^2+\omega_b^2,\\
a_3 =& \kappa_a\Delta_c^2+\gamma_b\left(\Delta_c^2+\frac{3\kappa_m^2}{2}+\tilde{\Delta}_m^2\right)+2g_{\rm ma}^2(\kappa_a+\gamma_b)\\
&+\sqrt{2}g_{\rm mb}Gm_s\omega_b+\frac{\kappa_a^3}{2}+\kappa_a\tilde{\Delta}_m^2+2\kappa_a\omega_b^2,\\
a_4 =& \frac{1}{2}g_{\rm ma}^2\left(-4\Delta_c\tilde{\Delta}_m+\kappa_a^2+4\kappa_a\gamma_b+4\omega_b^2\right)+\frac{1}{4}\kappa_m^2\\
&+\gamma_b\left(\kappa_a\Delta_c^2+\frac{\kappa_m^3}{2}+\kappa\tilde{\Delta}_m^2\right)+\Delta_c^2\omega_b^2+\Delta_c^2\tilde{\Delta}_m^2\\
&+g_{\rm ma}^4+\frac{3\kappa_a g_{\rm mb}Gm_s\omega_b}{\sqrt{2}}+\frac{\kappa_m^4}{16}+\frac{1}{4}\kappa_a^2\tilde{\Delta}_m^2+\tilde{\Delta}_m^2,\\
a_5 =& -2\Delta_c g_{\rm ma}^2\gamma_b\tilde{\Delta}_m+\sqrt{2}\Delta_c^2 g_{\rm mb}Gm_s\omega_b+\frac{1}{4}\kappa_a^2\\
&+\Delta_c^2\gamma_b\tilde{\Delta}_m^2+\kappa_a\Delta_c^2\omega_b^2+\sqrt{2}g_{\rm ma}^2g_{\rm mb}Gm_s\omega_b\\
&+\frac{1}{2}\kappa_a^2g_{\rm ma}^2\gamma_b+g_{\rm ma}^4\gamma_b+2\kappa_m g_{\rm ma}^2\omega_b^2+\frac{3\kappa_m^2g_{\rm mb}}{2\sqrt{2}}\\
&+\frac{1}{4}\kappa_m^2\gamma_b\tilde{\Delta}_m^2+\frac{\kappa_m^4\gamma_b}{16}+\kappa_a\tilde{\Delta}_m^2\omega_b^2+\frac{1}{2}\kappa_a^3\omega_b^2,
\end{aligned}$$

$$
\begin{aligned}
a_6 =& -2\Delta_c g_{\mathrm{ma}}^2 \tilde{\Delta}_m \omega_b^2 + \frac{\kappa_a \Delta_c^2 g_{\mathrm{mb}} G m_s \omega_b}{\sqrt{2}} + \frac{1}{4}\kappa_a^2 \\
&+ \Delta_c^2 \tilde{\Delta}_m^2 \omega_b^2 + \frac{\kappa_m g_{\mathrm{ma}}^2 g_{\mathrm{mb}} G m_s \omega_b}{\sqrt{2}} + \frac{1}{2}\kappa_a^2 g_{\mathrm{ma}}^2 \omega_b^2 \\
&+ g_{\mathrm{ma}}^4 \omega_b^2 + \frac{\kappa_m^3 g_{\mathrm{mb}} G m_s \omega_b}{4\sqrt{2}} + \frac{1}{4}\kappa_m^2 \tilde{\Delta}_m^2 \omega_b^2 .
\end{aligned}
$$

By applying the criterion to the coefficient matrix C, we obtain the stability criterion of the system, defined by the inequalities

$$
\Delta_n = \begin{vmatrix}
a_1 & a_0 & 0 & \vdots & 0 \\
a_3 & a_2 & a_1 & \vdots & 0 \\
a_5 & a_4 & a_3 & \vdots & 0 \\
\cdots & \cdots & \cdots & \cdots & \cdots \\
0 & 0 & 0 & \vdots & a_n
\end{vmatrix} > 0, \tag{a16}
$$

where n = 1-6. The stable and unstable parameter regimes are shown in Figure a2, and the parameters chosen in this paperwork are confirmed to be within the stable region.

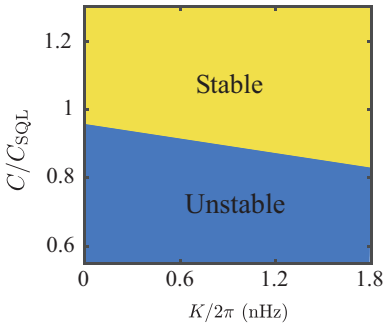

Figure a2 (Color online) The stable and unstable regions can be tuned by altering the magnon Kerr strength or the magnomechanical cooperativity, The parameters are the same as those in Figure 3.